Journal of Machine Engineering, Vol. 14, No. 2, 2014

orthogonal cutting,
burr, FEM simulation

Pawel PRES[1]
Waclaw SKOCZYNSKI[1]
Marek STEMBALSKI[1]

FINITE ELEMENT MODELLING OF BURR FORMATION IN METAL CUTTING

The paper presents a two-dimensional FEM model of burr formation in metal cutting. Abaqus/Explicit software was used for the build of the model. The workpiece geometry, the tool and the cutting parameters were modelled. Physical properties and the method of deformation and fracture of the workpiece material is described using Johnson Cook's constitutive law and the ductile damage criterion. The simulation of the edge formation process during orthogonal cutting was carried out for different depths of cut and cutting speeds. The results of these simulations allowed the verification of the FEM model. The components of the resultant cutting force measured during the actual cutting process with the values of these forces determined based on FEM simulation of this process were compared. The geometry of burrs formed during the actual and simulated the edge forming process was assessed. The analysis showed that the FEM model built enabled a correct prediction of the shape of the workpiece edge and the estimation of geometric features of the edge.

1. INTRODUCTION

The forming process of the workpiece edge in metal cutting is extremely complicated. Many factors contribute to this process. The most significant are: the type of machining, properties of the cutting material, workpiece geometry, feed rate, cutting speed, cutting depth, cutting tool geometry and the tool path [4]. Effective control of the burr formation process requires extensive analysis of the cutting process. It is necessary to be familiar with the interactions occurring between different parameters affecting the edge forming process. Many domestic and foreign research centers conduct research in this field. So far, this process has been widely analysed in regard to orthogonal cutting at low cutting speeds. Hashimura [1] introduced the workpiece edge forming process distinguishing eight key stages. He showed that the final shape of the workpiece edge significantly influences the direction of crack propagation, which leads to the creation of the burr. He distinguished two groups of materials: ductile and brittle and then made the direction of the propagation of this crack dependent on the properties of these materials. Current research in the field of fracture mechanics suggests that the method of fracture propagation leading to the creation of the

[1] Wroclaw University of Technology, Institute of Production Engineering and Automation, Poland,
E-mail: waclaw.skoczynski@pwr.edu.pl

burr, the mechanism of its creation, its type (shear or ductile) is dependent, among other things, on the stress triaxiality η [2],[3].

The aim of the study was the build of a two-dimensional FEM model of the workpiece edge shaping process and its extensive verification using the results of experiments carried out in accordance with the original methodology, which has been widely presented in [4],[11]. Based on the results of study [4],[11], the course of the FEM simulation of the workpiece edge forming process was compared to the actual course of this process. In addition, the components of the resultant cutting forces determined based on FEM simulation and measured during the experiment were analysed. A key element of the research was to compare the measurements results of geometric features of burrs formed during the experiment and in the FEM simulation. The research results presented in the papers [4],[11] have enabled a new approach to the verification of the FEM model of the workpiece edge forming process.

2. THE MODEL OF THE CUTTING PROCESS

The cutting process was modelled using the Abaqus/Explicit 6.9 EF software. For the discretization of the cutting tool, 666 finite elements type CPE4R were used. Their size decreased toward the tip of the cutting edge. For the discretization of the workpiece, 47502 finite elements type CPE4RT were used. The size of finite elements in a layer of the material being cut, with a constant concentration thereof, was the same. The length of the side of the finite element was equal to 0.01mm. The geometry of the workpiece, tool and the boundary conditions set are shown in Fig. 1. The workpiece was fixed using the base edge and the reference point, which was the pivot point of the workpiece. A *Coupling* type constraint was used.

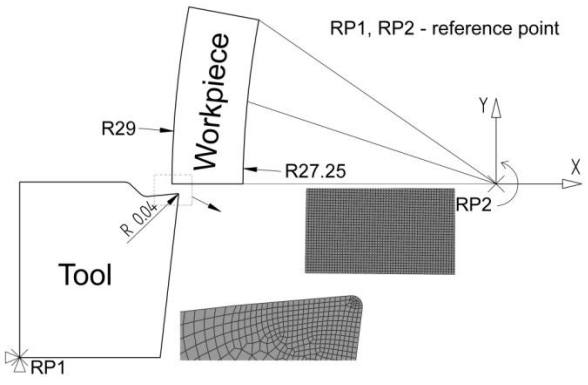

Fig. 1. Boundary conditions of the cutting process model

The front and end face of the workpiece has not been fixed. This way, free deformation of the workpiece edge was possible. The cutting tool has been firmly fixed by means of the reference point. A Rigid Body type constraint was used. The shape of the

modelled cutting edge corresponded to the actual one. Geometry measurements of the insert cutting edge were performed using a Form Talysurf 120L profilographometer made by Taylor Hobson. During the FEM simulation of the cutting process, the workpiece rotated around the Z-axis.

The phenomenon of friction between the material of the cutting tool and the workpiece material was modelled. Using the user subroutine VFRIC which is available in Abaqus/Explicit 6.9 EF software, the impact of sliding speed on the friction coefficient was taken into account. It was calculated according to the formula [5]:

$$\mu_t = 0.498 - 0.002 \times v_{ls} \tag{1}$$

where v_{ls} is the average local sliding speed. According to the study [5], the friction coefficient adopted values in the range $0.298 < \mu_t < 0.498$.

The user subroutine VUMAT which is available in Abaqus/Explicit 6.9 EF software was used to build a model of the workpiece material. The developed subroutine took into account the assumptions of the classic theory of elasticity and plasticity and continuum damage mechanics. Based on the hypothesis of "equivalent strain", constitutive equations taking into account the material stiffness degradation in the application of the Hook law were formulated, with the following form [6],[9],[10]:

$$\sigma = C^* \varepsilon \tag{2}$$

$$C^* = (1 - 0.3 \times D)\ C \tag{3}$$

where D is the parameter describing the material degradation. The increase of the equivalent plastic strain was calculated using the bisection method based on the relationship [7]:

$$\Delta\varepsilon^{pl} = \frac{\sigma_{eq} - \sigma_y}{3G} \tag{4}$$

where σ_{eq} is the equivalent von Mises stress calculated according to the formula [7]:

$$\sigma_{eq} = \sqrt{\frac{3}{2}(\sigma_{11}{}^2 + \sigma_{22}{}^2 + \sigma_{33}{}^2 + 2\sigma_{12}{}^2)} \times \frac{1}{1 - 0.3 \times D} \tag{5}$$

and σ_y is the yield stress, which was calculated on the basis of Johnson Cook's constitutive equation [8]:

$$\sigma_y = 1 - 0.3 \times D \quad A + B\ \varepsilon^{\ n}\ [1 + \ 1 - 0.3 \times D\ \frac{\varepsilon}{\varepsilon_0}]^C [1 - \frac{\theta - \theta_{room}}{\theta_{melt} - \theta_{room}}] \tag{6}$$

where: σ_y flow stress, ε^{pl} equivalent plastic strain, $\varepsilon^{\ pl}$ equivalent strain rate, ε_0 reference strain rate equal to 1 s^{-1}, A initial yield stress at a strain rate of 1 s^{-1} at the reference

temperature θ_{room}, B strain hardening coefficient, n strain hardening exponent, C strain rate dependency coefficient, m thermal softening exponent, θ current temperature, θ_{melt} melting temperature. Additional members $1 - 0.3 \times D$ of the equation (5) allowed to take into account the loss of the effect of strain rate hardening and strain hardening as well as the decrease in yield strength with the advancing material stiffness degradation [9],[10],[12]. On the basis of the data presented in the literature the values of the parameters of Johnson Cook's constitutive model and the values of constants that describe the physical properties of the workpiece were selected (Table 1).

Table 1. The values of the parameters of Johnson Cook's equation and physical properties of steel C45E (units in accordance with their system adopted in the Abaqus system) [11]

Young Modulus E (MPa)	Poisson Ratio v	Density ρ (ton/mm^3)	Specific Heat C_p (mJ/ton °C)	Conductivity T_c (mW/mm °C)	Room temperature θ_{room} (°C)
210000	0.3	7.821e-09	452e9	48.1	20
Yield stress A (MPa)	Hardening modulus B (MPa)	Strain rate dependency coeff., C	Work hardening exponent n	Thermal softening coefficient m	Melting temperature θ_{melt} (°C)
375	552	0.02	0.457	1.4	1460

The mechanism of fracture initiation and propagation of the material was taken into account using the ductile damage criterion [7]. It was assumed that the equivalent strain at fracture ε_0^{pl} depends on the non-dimensional value of the stress traxiality η and the strain rate ε^{pl}. Initiation of material degradation $(\omega = 1)$ occurred when the limit value of plastic strain was reached:

$$\omega = \frac{d\varepsilon^{pl}}{\varepsilon_0^{pl}\ \eta, \varepsilon^{pl}} = 1 \tag{7}$$

The value the equivalent strain at fracture ε_0^{pl}, on which the initiation of the loss of material stiffness depended, was calculated from the relation [12],[13]:

$$\varepsilon_0^{pl} = (0.465e^{-1.96\eta})(1+\varepsilon)^{0.0018} \tag{8}$$

The fact was taken into account that, as shown in [3], cracking does not occur for value of stress triaxiality η less than or equal to -1/3.

At the moment of reaching the value of equivalent plastic strain at fracture ε_0^{pl} according to the relation (7) and the fulfilment of the initiation condition $(\omega = 1)$, a gradual degradation of the material stiffness took place $(D \Rightarrow 0.99)$ until the loss

of coherence and removal of the finite element ($D = 0.99$). The degree of degradation was determined from the relation [7],[14]:

$$D = \frac{\int_{\varepsilon_0^{pl}}^{\varepsilon_f^{pl}} L\sigma_y d\varepsilon^{pl}}{G_f} = \frac{\int_0^{u^{pl}} \sigma_y du^{pl}}{G_f} \tag{9}$$

where: L is the characteristic length of the finite element and G_f is the fracture energy. The fracture energy value was equal to 8. This value was adopted on the basis of the simulation of the cutting process (e.g., the method of forming a chip) and the components of the resultant cutting forces measured during the simulation.

In addition, a parameter η_s was introduced, determining the average rate of change of the stress triaxiality value in the course of two successive calculation steps. The value of the η_s parameter was calculated according to the formula:

$$\eta_n = \frac{abs(\eta_n - \eta_{n-1})}{dt} \tag{10}$$

$$\eta_{n+1} = \frac{abs(\eta_{n+1} - \eta_n)}{dt} \tag{11}$$

$$\eta_s = \frac{\eta_{n+1} + \eta_n}{2} \tag{12}$$

where the indices n, n-1, n +1 denote the number of increment. Finally, the value of the equivalent strain at fracture was calculated according to the following formula:

$$\varepsilon_0^{pl} = \begin{array}{ll} (0.465e^{-1.96\eta})(1+\varepsilon)^{0.0018} & for \quad \eta_s \leq 5000 \wedge \eta > -1/3 \\ \infty & for \quad \eta_s \geq 5000 \vee \eta < -1/3 \end{array} \tag{13}$$

3. SIMULATION OF THE CUTTING PROCESS

Using the FEM model built, a simulation of the cutting process was performed using different machining parameters. Cutting speed v_c was equal to 180, 220 and 280m/min. Depth of cut a_p was equal to 0.1, 0.15, 0.2, 0.3mm. The course of the simulated workpiece edge forming process is shown in Fig. 2. Similarly to the actual workpiece edge forming process a breakout type burr was obtained. The successive stages of the process were also correctly modelled. Some differences were observed with respect to the direction of crack propagation. In actual burr formation, a crack propagates at an angle relative to the direction of the main component of the resultant cutting force [4],[11]. In the modelled workpiece edge forming process the crack propagated along the direction of the main component of the resultant cutting force, until a significant deformation of the material at the edges occurred.

Figures 3 and 4 show the distributions of values of equivalent plastic strain (*PEEQ* parameter in the Abaqus system) and temperature, which can be observed in the course of numerical simulation. The observed values of the equivalent plastic strain for finite

elements located in the cutting zone ranged from 1 to 3. The temperature distribution visible in Fig. 4 and its high values may indicate that there is too large strain of the modelled material (based on a well-known fact that by far the most heat during the cutting process arises as a result of plastic deformation).

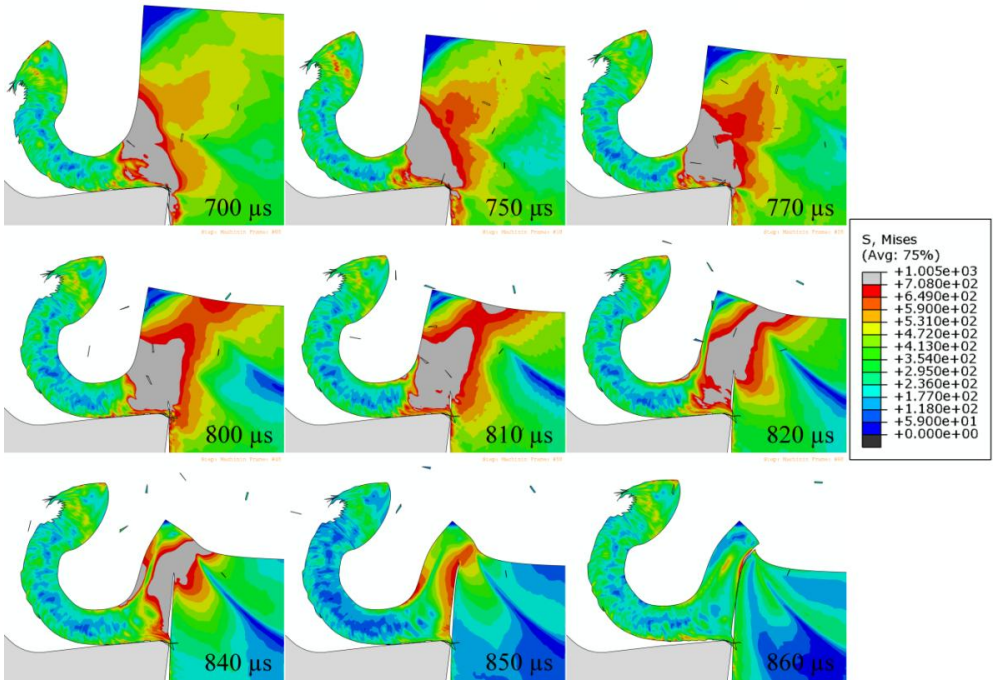

Fig. 2. Distribution of the equivalent von Mises stress during FEM simulation of the burr forming process at the workpiece edge (a_p = 0.2mm, v_c = 280m/min)

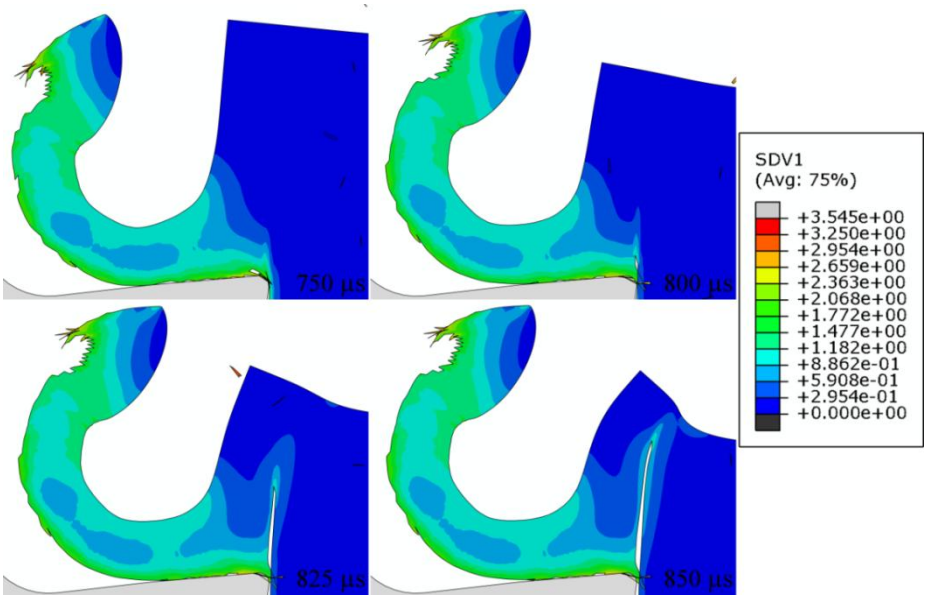

Fig. 3. Distribution of equivalent plastic deformation (PEEQ) during FEM simulation of the burr forming process (a_p = 0.2mm, v_c = 280m/min)

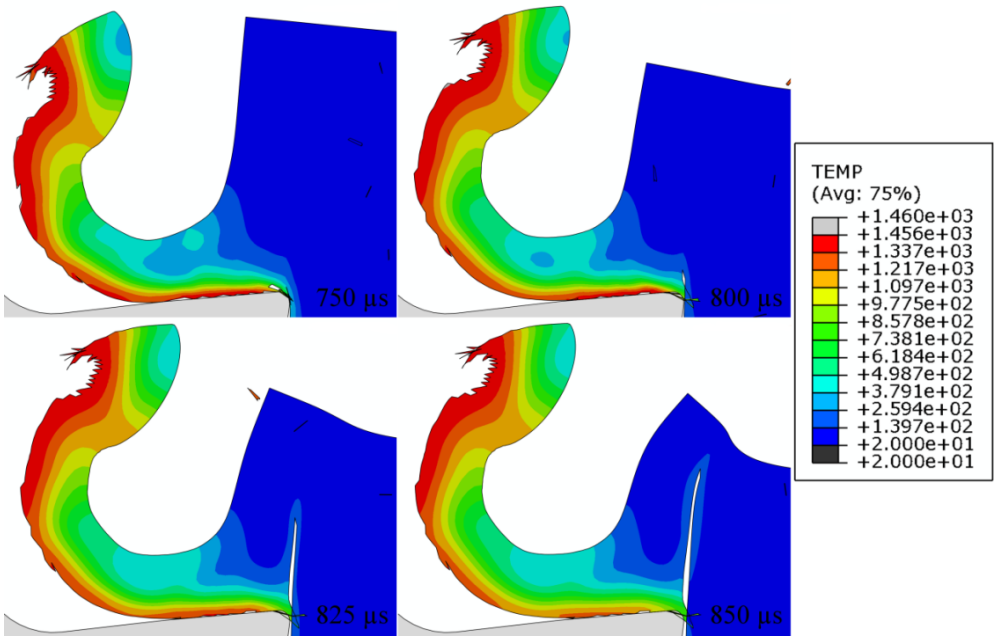

Fig. 4. Temperature distribution during FEM simulation of the burr forming process (a_p = 0.2mm, v_c = 280m/min)

4. VERIFICATION OF THE CUTTING PROCESS MODEL

In order to verify the accuracy of the FEM model built, the values of cutting force components measured during the actual and simulated orthogonal cutting were compared (Fig. 5 and 6). Based on statistical analysis (residual variance values S_e^2 were compared), it

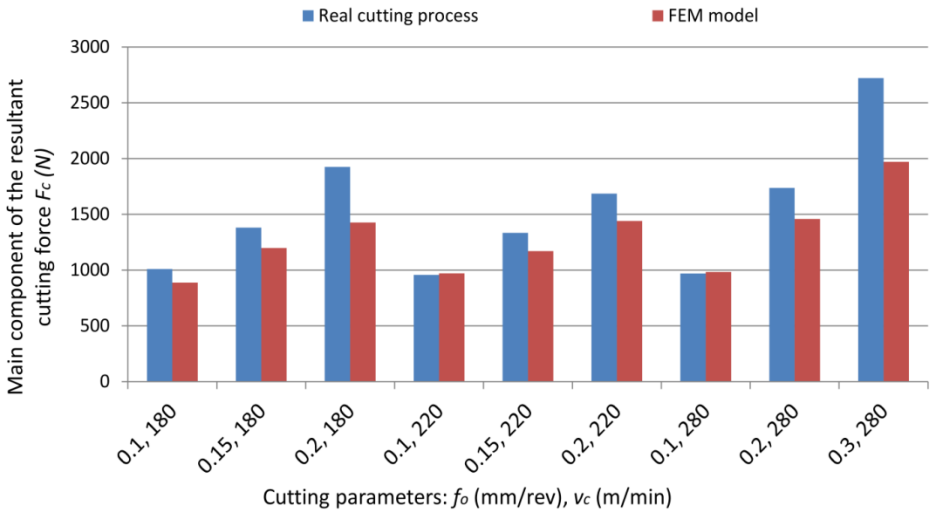

Fig. 5. Comparison of the value of the main components F_c of the resultant cutting force depending on the value of feed f_o (mm/rev) and cutting speed v_c (m/min) measured during the actual process of cutting and determined in the FEM model simulation

was estimated that the accuracy of forecasts of the main cutting force component was higher than the feed component of the cutting force. A measure of the quality of matching the forecast results of the components of the resultant cutting force to the experimental data (coefficient of determination R^2) was equal to 0.69. Relative error in the case of the forecast of the value of the main component of the resultant cutting force F_c ranged from 1.4 to 27.6% of the value measured experimentally. The error value increased with the value of force. The highest accuracy of the estimate of the main component was obtained for feed equal to 0.1mm/rev. Forecast error of the feed component of the cutting force F_f was equal to from 38.9 to 69.5%.

Further, the geometric features of the edges formed during the actual and simulated cutting process were analysed. The values of the parameters defining the geometric features of these edges were compared, such as burr height a, burr decrease c, burr length b (Fig. 7).

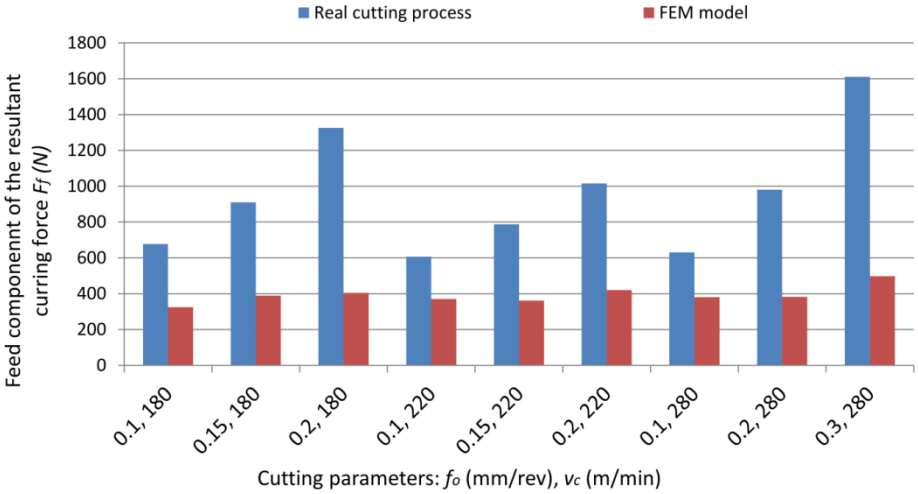

Fig. 6. Comparison of the value of the feed components F_f of the resultant cutting force depending on the value of feed f_o (mm/rev) and cutting speed v_c (m/min) measured during the actual process of cutting and determined in the FEM model simulation

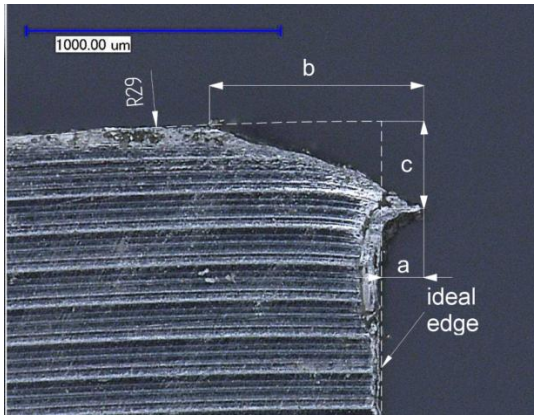

Fig. 7. Measurement method for selected geometric features of the burr

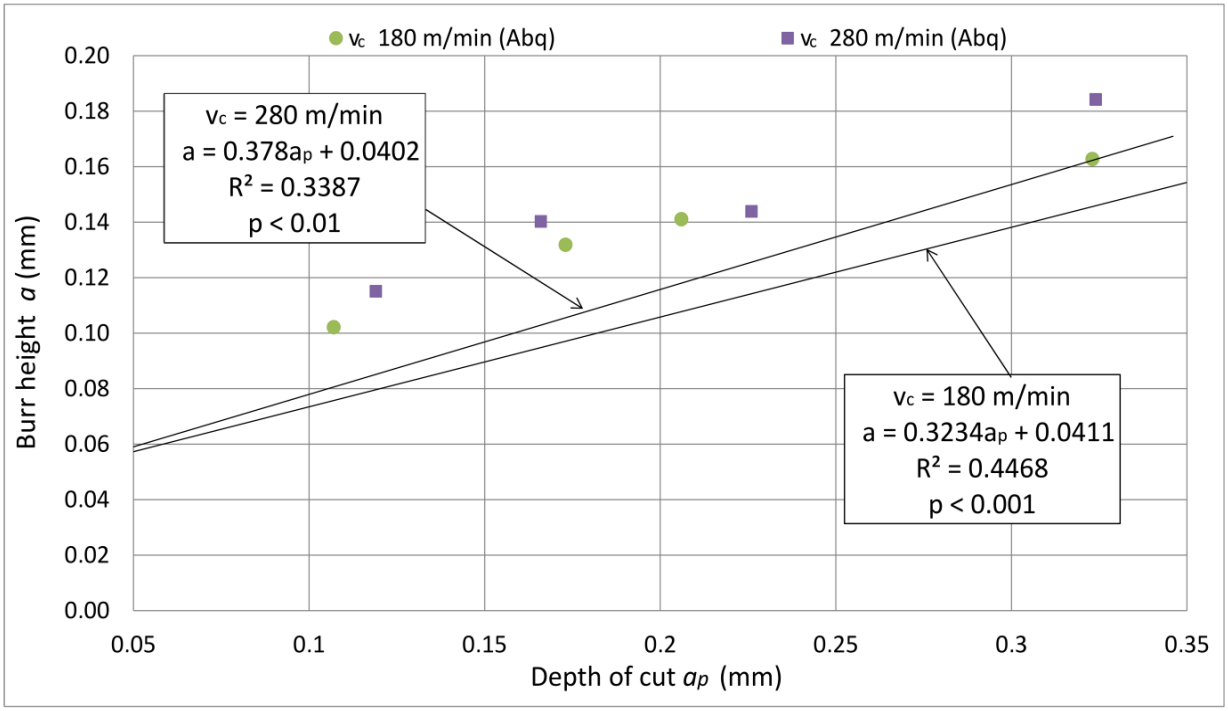

Fig. 8. Dependence of the height of burr a on the cutting depth a_p. Comparison of experimental results (trend lines) and FEM simulations (points)

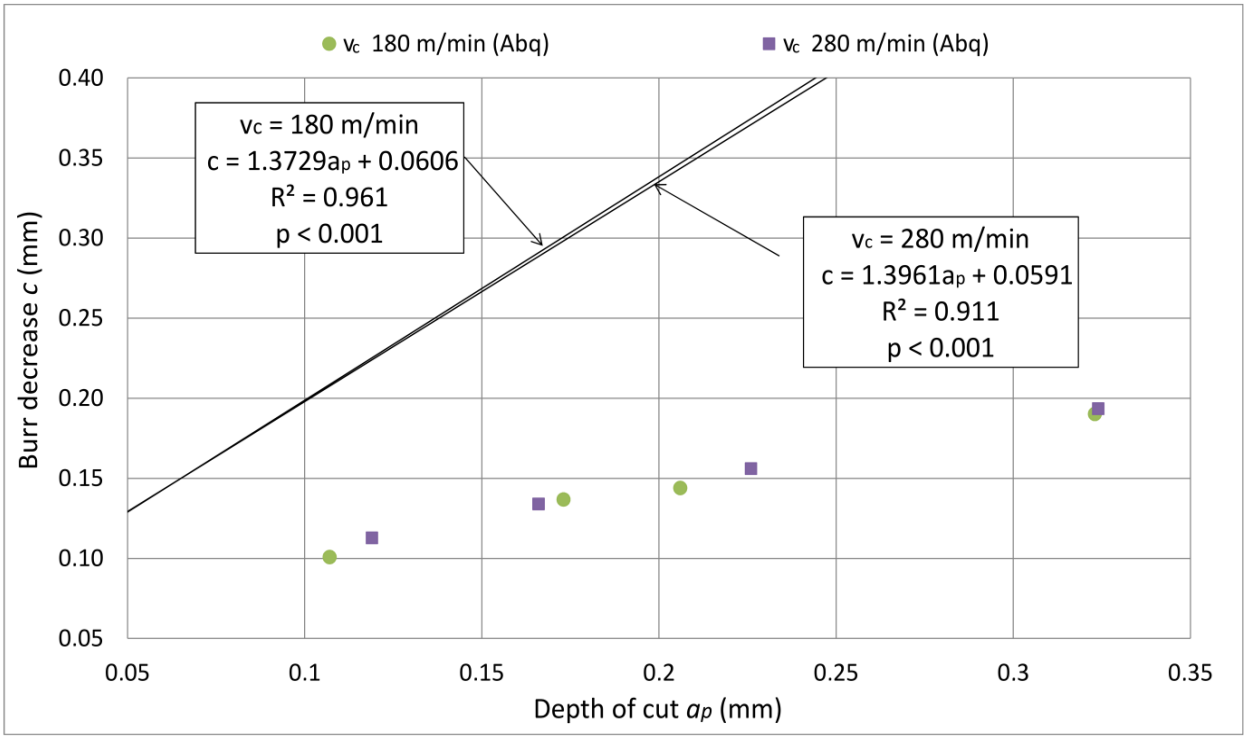

Fig. 9. Dependence of the reduction of burr b on the cutting depth a_p. Comparison of experimental results (trend lines) and FEM simulations (points)

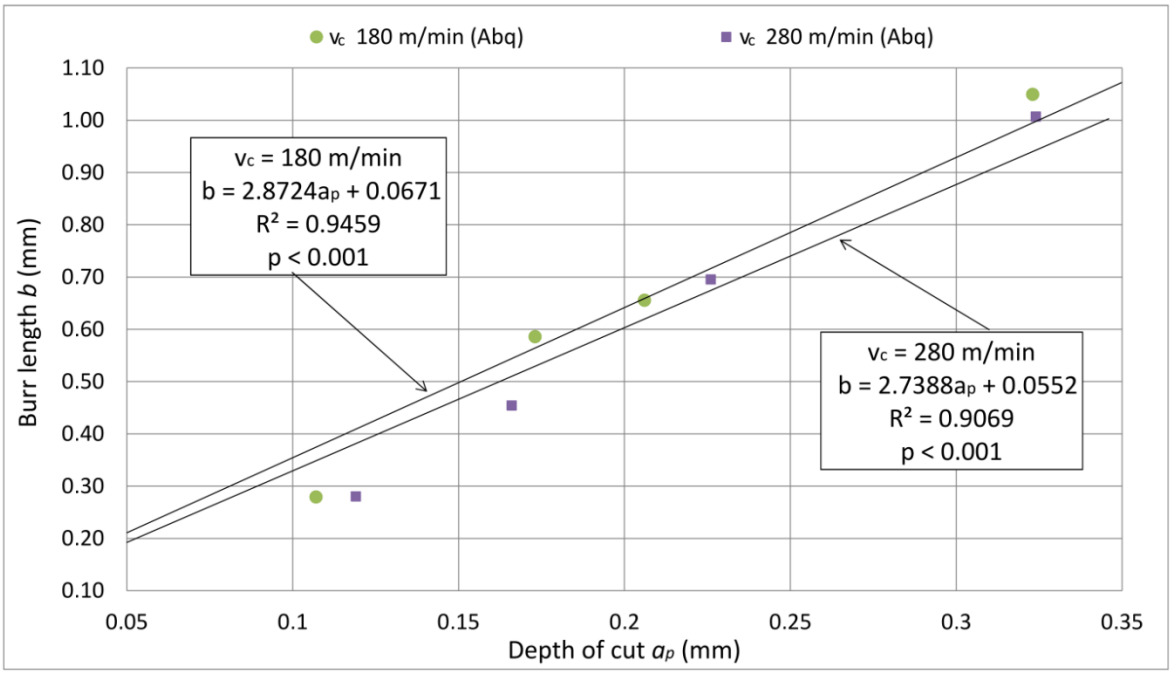

Fig. 10. Dependence of the length of burr *b* on the cutting depth a_p. Comparison of experimental results (trend lines) and FEM simulations (points)

Figures 8, 9 and 10 show, in the form of comparison, the results of measurements of geometric features of burrs obtained during experimental studies (trend lines) [4],[11] and during the FEM model simulations (points). The dependence of selected geometric features of the burr *a*, *b*, *c* on depth of cut a_p and cutting speed v_c were shown. The average value of the relative error for the forecast of values for parameter *a* was 27%, for parameter *b* 10% and for parameter *c* 56%.

5. CONCLUSIONS

Based on a comparison of the simulated and the actual process of workpiece edge forming, the following conclusions were made:

1. The FEM model enabled the estimation of the components of the resultant cutting force that occurring during machining of steel C45E in terms of the cutting parameters used.
   A very good agreement with the results of the experiment was obtained in terms of the main component of the cutting force, whereas the values of the feed component were underestimated.
2. The FEM model of the material deformation process at the workpiece edge during orthogonal cutting enabled the correct forecast of the workpiece edge forming process and the shape of the burr in regard to the analysed machining parameters and the estimation of the values of the parameters defining the selected geometric features of the burr.

3. The direction of crack propagation in the initial stage during the actual forming process of the burr was inclined at an angle to the direction of relative movement of the tool. In contrast, during the FEM simulation of the burr forming process, the propagation direction was parallel to the relative movement of the tool. As a result, the value of burr decrease *c* was calculated on the basis of the simulation shown was underestimated compared to the experimentally determined value.

ACKNOWLEDGEMENTS

The computations were performed on the computers of the Wroclaw Centre of Networking and Supercomputing (http://www.wcss.wroc.pl), computing grant no. 178.

REFERENCES

[1] HASHIMURA M., HASSAMONTR J., DORNFELD D., 1999, *Effect of in-plane exit angle and rake angles on burr height and thickness in face milling operation*, Journal of Manufacturing Science and Engineering, 121/1, 13–19.
[2] XUE L., WIERZBICKI T., 2008, *Ductile fracture initiation and propagation modeling using damage plastic theory*, Engineering Fracture Mechanics, 75, 3276–3293.
[3] BAO Y., WIERZBICKI T., 2005, *On the cut-off value of negative triaxiality for fracture*, Engineering Fracture Mechanics, 72, 1049–1069.
[4] PRES P., SKOCZYNSKI W., JASKIEWICZ K., 2014, *Research and modeling workpiece edge formation process during orthogonal cutting*, Archives of Civil Mechanics and Engineering (in press), http://dx.doi.org/10.1016/j.acme.2014.01.003
[5] RECHT J., CLAUDIN C., D'ERAMO R., 2009, *Identification of a friction model application on the context of dry cutting of an AISI 1045 annealed steel with a TiN-Coated carbide tool*, Tribology International, 42, 738–744.
[6] ZHONG W., CAI Y., 2011, *Continuum damage mechanics and numerical application*, Springer Berlin Heidelberg.
[7] Abaqus 6.9EF software documentation.
[8] JOHNSON G.R., COOK W.H., 1983, *A constitutive model and data for metals subjected to large strains, high strain rates and high temperatures*, In Proceedings of the 7th International Symposium on Ballistics, 541–547.
[9] BORVIK T., HOOPERSTAND O.S., BERSTAD T., LANGSETH M., 2001, *A computational model of viscoplasticity and ductile damage for impact and penetration*, Eur. J. Mech. A/Solids, 20, 685–712.
[10] BORVIK T., HOPPERSTAD O.S., BERSTAD T., 2003, *On the influence of stress triaxiality and strain rate on the behavior of a structural steel. Part II. Numerical study*, European Journal of Mechanics A/Solids, 22, 15–32.
[11] PRES P., 2013, *Research and modelling phenomenon of burr formation at the edge of the workpiece* (in Polish), PhD thesis, Wroclaw University of Technology, Institute of Production Engineering and Automation.
[12] ABUSHAWASHII Y., XIAO X., ASTAKHOV V., 2011, *FEM simulation of metal cutting using a new approach to model chip formation*, International Journal of Advances in Machining and Forming Operations, 3/2, 71–92.
[13] MABROUKI T., RIGAL J., 2006, *A contribution to qualitative understanding of thermo mechanical effects during chip formation in hard turning*, Journal of Materials Processing Technology, 176, 214–221.
[14] HILLERBORG A., MODEER M., PETERSSON P.E., 1976, *Analysis of crack formation and crack growth in concrete by means of fracture mechanics and finite elements*, Cement and Concrete Research, 6, 773–782.